Magnetism in nanoscale graphite flakes as seen via electron spin resonance

Luka Ćirić, Dejan M. Djokić,* Jaćim Jaćimović, Andrzej Sienkiewicz, Arnaud Magrez, and László Forró
Ecole Polytechnique Fédérale de Lausanne, ICMP, 1015 Lausanne, Switzerland

Željko Šljivančanin
Vinča Institute of Nuclear Sciences (020), RS-11001 Belgrade, Serbia

Mustafa Lotya and Jonathan N. Coleman
School of Physics, Trinity College Dublin, Dublin 2, Ireland
(Received 7 March 2012; published 22 May 2012)

Magnetic properties of a large assembly of ultrathin graphitic particles obtained by heavy sonication of graphite powder dispersed in *N*-methylpyrrolidone were measured by electron-spin resonance (ESR). The ESR signal was decomposed into one narrow and one broad component. The narrow component was associated with localized Curie-type defects. The temperature dependence of the predominant broad component points to a transition to a superparamagnetic-like state at 25 K. By performing the density-functional-theory calculations for graphene with selected extended defects (the sheet edges, zigzag chains of chemisorbed H atoms, and pentagon-octagon rows), we found considerable magnetic moments at C atoms in their vicinities. We attribute the magnetism in the graphitic particles to the localized electronic states near the defects in the network of the π electrons of graphene. The ferromagnetic (FM) correlations among magnetic moments at carbon atoms near the edges are not able to give rise to a long-range FM order.

DOI: 10.1103/PhysRevB.85.205437 PACS number(s): 73.22.Pr, 75.70.Cn, 73.20.−r, 76.30.Pk

I. INTRODUCTION

After fullerenes and carbon nanotubes, the interest in an *old* polymorphism of carbon, graphene, is strongly increasing. This interest is due to the ease of its production and to the nonsophisticated theoretical modeling of its electronic structure. However, despite these simplicities graphene has many attractive features both in basic science and in applications. One of these possibilities is to use it in spintronics.[1] Theoretical modeling has shown that the localized states at the edges of graphene nanoribbons can have a long-range magnetic order, and as such, they can carry the spin information.[2] Furthermore, Son *et al*.[3] have predicted that the opposite edges have opposite spin configurations which could be tuned by electric field. This gives an additional control of the information transport.

Despite these spectacular theoretical predictions, the experimental demonstration of this long-range spin order in graphene and in graphene nanoribbons is still missing.[4] Very recent findings stemming from muon spectroscopy[5] have also eliminated the possibility of the formation of ferromagnetic (FM) or antiferromagnetic (AFM) ordering in defective graphene. Nevertheless, it has generated the revival of the investigation of ferromagnetism in graphite and in other carbon-based materials (CBMs). Already, the search for magnetism in CBMs has a long tradition. The interest was always to create nanoscale magnetic and spin-electronics devices. The light weight and the abundance of carbon would make CBMs ideal candidates, but one would need a FM state at room temperature (RT). There are only a few CBM ferromagnets, but their Curie temperatures (T_C) are well below RT. One prominent example is TDAE-C_{60} with a T_C of 12 K.[6] The FM state has been shown to be very fragile, depending on the thermal history of the sample. The exchange interaction (J) of the localized wave function of the electron on the C_{60} gives rise to a FM state only in a special mutual configuration of the molecules because J depends on the overlap between adjacent sites.[7]

Most of the CBM-related ferromagnetism is reported for graphite and attributed to the presence of impurities or lattice imperfections like cracks, grain boundaries, and voids. Electron- and ion-irradiation-induced defects in graphite also can result in a FM state.[8] The underlying model in these cases relies on the defect-induced localized states at the Fermi level, leading to the existence of local moments. If these defects are aligned, e.g., on a grain boundary, direct exchange can give a FM state with a rather high T_C.[9] If the local moments are dispersed in space, then the Ruderman-Kittel-Kasuya-Yosida (RKKY) interaction is evoked for aligning the spins.[10] Nevertheless, in this case the T_C is rather low. Furthermore, it is debated in the literature whether the low carrier concentrations in CBMs, especially in graphene, are capable of producing sizable RKKY couplings between the localized spins.[11]

A mean-field theoretical study, carried out for randomly distributed magnetic defects in graphene,[12] has reported that FM correlations can coexist alongside an AFM exchange. On the other hand, the presence of AFM correlations in a magnetic phase induced by nonmagnetic structural defects in a single graphene sheet still remains less likely. This is because the antiferromagnetic-spin arrangements occur at special edge-defect configurations, such as edge segments separated by the turn of 120°.[13]

Our work is a study of magnetism of nanographite with the philosophy that a deeper understanding of ferromagnetism in ultrathin graphitic systems will help to transfer this knowledge to graphene ribbons and to be useful in its spintronics applications. We report the detection of a superparamagnet-like state below 25 K in an assembly of nano-sized graphitic particles. These particles were created with a heavy sonication of graphitic powder in *N*-methylpyrrolidone (NMP). The

mechanical shock of the nanoparticles could produce structural defects which strongly perturb the electronic structure within graphene layers. The defect density, however, is not overwhelming; otherwise, the Raman study would notice it.[14]

The monoatomic-carbon vacancies are the simplest structural defects able to induce magnetism in graphene. We assume that the magnetism observed in the experiments described in this manuscript originates from structural imperfections more complex than monoatomic vacancies. Employing *ab initio* calculation, we identified several line defects which give rise to the magnetism in graphitic particles. The set of investigated defects includes the graphene edges, intrinsic structural defects in the honeycomb lattice, and zigzag chains of adsorbated H atoms. The calculations demonstrate that the emergence of defects in the π network of valence electrons gives rise to nonzero-spin density in a graphene sheet.

II. METHODS

A. Experiment

The nanographite sample was obtained as a by-product of graphite exfoliation in order to produce high-quality graphene.[15] A sieved graphite powder was dispersed in *N*-methylpyrrolidone by bath sonication. After sonication for 30 minutes, a gray liquid was obtained consisting of a large number of graphitic particles, including graphene flakes. The assembly was drawn through a filter paper, and a thick black deposit was obtained. Its characterization by scanning electron microscopy (SEM) is shown in Fig. 1. Most of the graphitic flakes are flat on the filter paper. A particle counting shows that more than 70% of the flakes have surface areas $\leqslant 1\ \mu m^2$, and roughly 2% are $\geqslant 50\ \mu m^2$.

The predominance of submicron-sized particles justifies the denomination *nanographite*. We do not have real statistics about the thicknesses of these particles, but independent study has shown that it contains a large number of graphene flakes.[15] The electron-spin-resonance (ESR) silent filter paper with the graphitic deposit was cut into $3.0 \times 5.0\ mm^2$ rectangles, and approximately ten of them were piled up and introduced into an ESR quartz tube which was evacuated, filed with 100 mbar of high-purity Helium gas, and sealed.

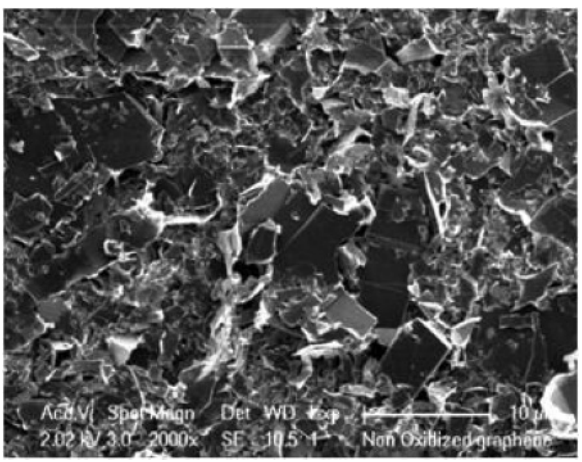

FIG. 1. Scanning-electron-microscopy (SEM) image of the large assembly of graphitic particles. At least 66% of the particles have a surface area $\leqslant 1\ mm^2$.

B. Theory

In order to examine prospects for defect-introduced magnetism in graphitic nanoparticles, we perform calculations of the electronic properties of graphene flakes and an infinite graphene layer with selected structural imperfections. The theoretical investigations are restricted to the structures containing a single graphene layer since the weak van der Waals forces between graphene sheets are not expected to substantially alter their magnetic properties. The structures considered in the present study are depicted in Fig. 2. The rationale which led to this choice of investigated structural defects in graphene is described in the next section together with the corresponding density-functional-theory (DFT) results.

All calculations are performed with the GPAW computer program[16,17] based on the real-space implementation of the projector-augmented-wave (PAW) method.[18] The electronic-exchange-correlation effects are described applying a Perdew-Burke-Ernzerhof exchange-correlation functional.[19] We used the grid spacing of 0.15 Å. The calculations for the graphene flake in Fig. 2(a) are performed employing open-boundary

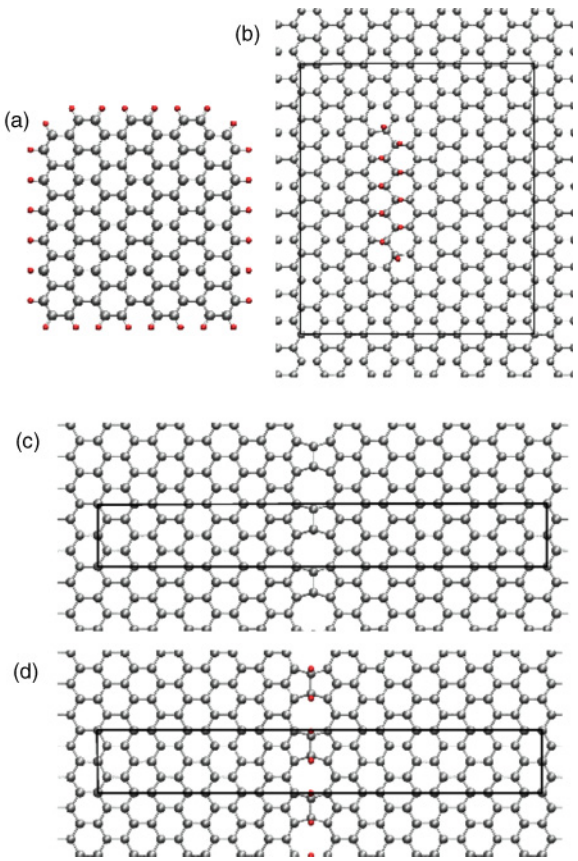

FIG. 2. (Color online) The atomic structure of (a) a small rectangular graphene flake, (b) a zigzag line of H adatoms on graphene, (c) a bare line defect containing carbon pentagons and octagons, and (d) a hydrogenated-line defect containing carbon pentagons and octagons. The H and C atoms are represented by red and gray spheres, respectively. For structures in (b)–(d), the surface unit cells are marked with black lines.

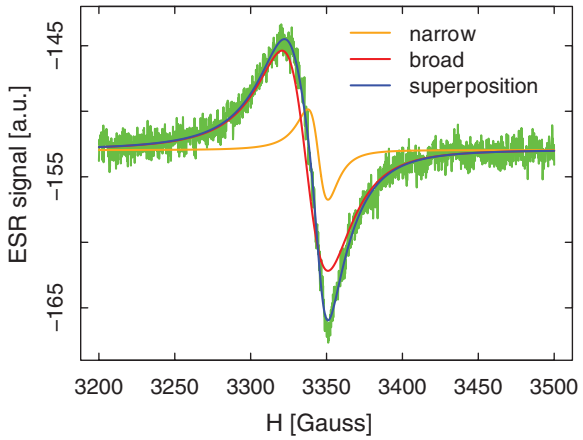

FIG. 3. (Color online) A typical ESR signal of the nanographite sample recorded at 100 K. The asymmetric signal is well fitted with a narrow and a broad component. The resonance field was roughly in the $H_0 \perp c$ configuration.

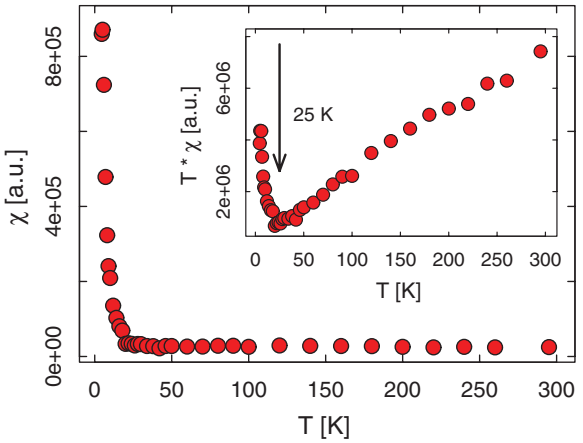

FIG. 4. (Color online) The temperature dependence of the spin susceptibility corresponding to the broad component of the ESR line. The inset depicts the strong increase of both χ and $\chi * T$ below 25 K points to the onset of magnetic interactions.

conditions. The H chains [Fig. 2(b)] and extended-line defects [Figs. 2(c)–2(d)] are examined using the supercell approach and applying periodic-boundary conditions in the graphene plane. The corresponding Brillouin zones are sampled with one (chains of H adatoms) and 16 Monkhorst-Pack **k** points (extended-line defects).

III. RESULTS

A. Experiment

At high temperatures the signal is Lorentzian while below 150 K it becomes asymmetric. An example of the signal recorded at 100 K is shown in Fig. 3. It can be fitted with two Lorentzian-absorption profiles as a sum of a broad and of a narrow component.

The narrow line could be followed up to 150 K. Its intensity obtained by the double integration of the ESR line is proportional to the spin susceptibility (χ) and shows a Curie behavior ($\chi \sim 1/T$).

It is worth mentioning that ESR spectra originating from conduction electrons are often asymmetric (Dysonian type). This effect is also observed in graphite and graphite-intercalation compounds (GIC)[20] but not in our sample consisting of nano-sized graphitic particles, and we will not discuss that matter in this paper.

The double-integrated broad line gives a Pauli-like susceptibility as in most of the graphite samples. This resemblance breaks at 25 K where the spin susceptibility starts to increase strongly on cooling (Fig. 4). This increase cannot be attributed simply to the appearance of a Curie tail since this increase is abrupt and much stronger than $\sim 1/T$.

This could be easily seen in the inset of Fig. 4 where the $\chi * T$ plot shows diverging behavior below 25 K, strongly suggesting the onset of FM correlations.

The g factor and the ESR linewidth (Fig. 5) corroborate with the behavior of the spin susceptibilities.

For the narrow-line component they reveal both the value and the featureless temperature dependence which is similar to that observed for defects in CBMs. However, the defects in our sample are not exactly the same as those observed in electron- or ion-irradiated samples,[21] whose g factors are close to the free-electron value of 2.0023. In our case the g factor is higher (2.006), resembling the defects created by incomplete functionalization, e.g., oxidation or reduction.[22] The augmented g value could be observed for the broad component as well. In graphite in the static-resonance magnetic-field configuration H_0 parallel to the c axis, g has a strongly temperature-dependent value starting from 2.05 at 300 K and reaching 2.15 at 25 K.[23] In our nanographitic sample the g value is 2.011 at RT and shows practically no temperature dependence down to 25 K. At this transition g sharply decreases as the consequence of the onset of an internal magnetic field.

B. Theory

To investigate the possibility of the magnetism in graphene induced by structural imperfections more complex than monoatomic vacancies, we focus on three types of line defects depicted in Fig. 2: hydrogenated zigzag graphene edges, a zigzag chain of H adatoms at graphene, and a bare or hydrogenated intrinsic graphene line defect containing rows

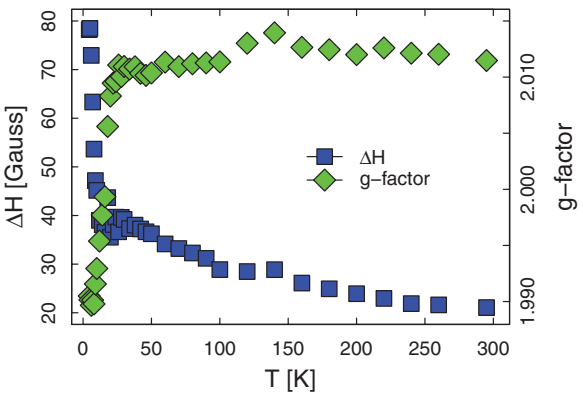

FIG. 5. (Color online) The ESR linewidth (left axis) and g factor (right axis) of the broad component of the ESR line as a function of temperature. At 25 K both quantities show the onset of magnetic correlations.

of carbon pentagons and octagons. All these defects can be modeled at modest computational cost applying DFT calculations and give rise to the zigzag boundaries in the π network of graphene valence electrons. Hence, these defects open the prospect for producing the spin-polarized-electron density in graphene following the same mechanisms described by Son *et al*. for zigzag graphene nanoribbons.[24]

The graphene edges are inevitable in any graphene sample of a finite size. Their effect on magnetism is modeled considering a nearly squared graphene nanoparticle in Fig. 2(a) since the majority of graphitic particles observed by SEM (Fig. 1) are of similar shapes. The DFT calculations of graphene flakes reveal that nonvanishing spin density is mostly located at C atoms near zigzag edges. The magnetic moment at the atoms along the same zigzag edge are ferromagnetically coupled with different signs for atoms near different zigzag edges [see Fig. 6(a)].

Thus, regarding ground-state magnetic properties, the graphene flake in Fig. 2(a) could be considered as a finite graphene nanoribbon.

The zigzag lines of H adatoms on graphene in Fig. 2(b) are among the favorable adsorption configurations of small hydrogen clusters on graphene[25] and, hence, could be produced during the process of graphite sonication in NMP. We examined the possibility to induce magnetism in graphene in the vicinity of the H-chain structure in Fig. 2(b) and found magnetic moments of $\sim$0.3 μ_B at C atoms near H adsorbates. The most favorable magnetic configuration corresponding to the H-zigzag chain on graphene is presented in Fig. 6(b).

The octagon-pentagon lines [Fig. 2(c)] are some of the simplest extended intrinsic line defects in graphene. They have been recently observed by Lahiri *et al*.,[26] who combined scanning transition microscopy (STM) with DFT calculations to resolve their structure at the atomic level. According to our calculations, negligible spin polarization occurs in the bare lines of pentagons and octagons. However, the picture changes significantly when the H atoms are adsorbed at line defects as depicted in Fig. 2(d). For the H-adsorption configuration in Fig. 2(d), we calculated the binding energy of 2.49 eV per H atom. This value is 0.78 eV higher than that for H chains of defect-free graphene.[27] Thus, the line defect is likely to be hydrogenated if the source of H atoms is available. The spin-density plot in Fig. 6(c) clearly demonstrates that the hydrogenated-line defect induces significant magnetic moments at C atoms in its vicinity. The magnetic moments are ferromagnetically coupled, giving rise to the total magnetic moment of 1.22 μ_B per unit cell.

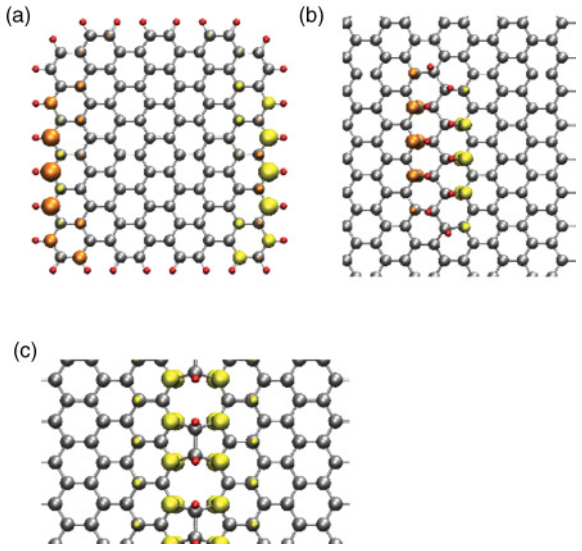

FIG. 6. (Color online) The isocontour plots of spin densities of (a) a small rectangular graphene flake, (b) a zigzag line of H adatoms on graphene, and (c) a hydrogenated-line defect containing carbon pentagons and octagons. Yellow and orange colors are used to represent spin densities generated from electron states with opposite spin orientations.

IV. DISCUSSION

The narrow line represents only $\sim$2% of the total intensity of the ESR signal. We attribute it to impurities in the sample. Its g factor and linewidth resemble the defects in graphene obtained by reduction of graphene oxide,[22] so we cannot exclude that they are situated in the exfoliated graphene flakes. Since there is no marked temperature evolution of this signal, we will disregard its further discussion.

The broad line coming from the majority phase shows in all physical quantities: intensity, linewidth, and g factor of the onset of the FM phase at 25 K. It manifests in the strong increase of the spin susceptibility and linewidth and in the abrupt decrease of the resonance field. Although these quantities show the appearance of a FM phase in the available temperature range, no long-range order emerges. The ESR line is still observable around a value of $g = 2$. This is explained by a FM transition in small domains at 25 K without interdomain interaction, and they could be considered as superparamagnetic clusters. They give an enhanced susceptibility and ESR-line broadening due to the distribution of local internal fields.

Since such a FM signal is absent in the graphite powder before sonication in NMP, the structure hosting the FM interaction was necessarily created during this procedure. One can suppose that the sonication creates defects such as vacancies or chemical functionalization. The model which accounts in this case for the FM state was elaborated by Yazyev and Helm.[28] It is based on the experimental STM observations[29] that a defect on a graphite surface causes the perturbation of the electronic structure in a large region. One can trace distinctive triangular patterns associated with individual quasilocalized states.[29] Evoking Lieb's theorem,[30] which relates the total magnetic moment of a half-filled bipartite system to the difference of the number of defects in the two sublattices, they could account for the FM signal in defected CBM systems. However, Lieb used the words *unsaturated ferromagnetism* to clarify that there is no spatial ordering.

An important question is the nature of the defects on the surface of nanographite, giving the local magnetic order. It is likely that they are extended defects which are created by the mutual shocks of the graphitic particles during the sonication. If the defects of different surface densities are produced in complementary sublattices not too close to each other, they show an enhanced magnetic moment. This is the scheme for ferromagnetism depicted in Refs. 28 and 31. However, based

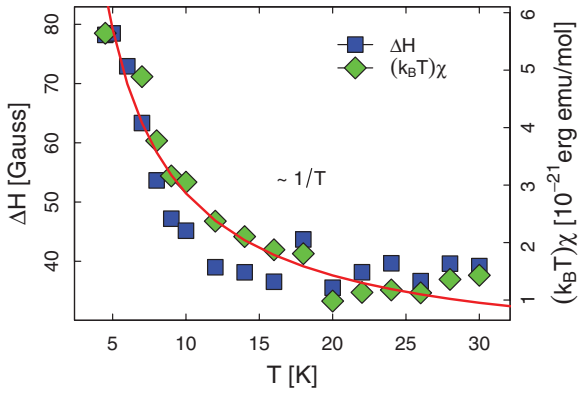

FIG. 7. (Color online) The linewidth and (k_BT)-multiplied susceptibility at low temperatures. The red curve represents the best fit $(\sim 1/T)$ for both mutually scaling dependences.

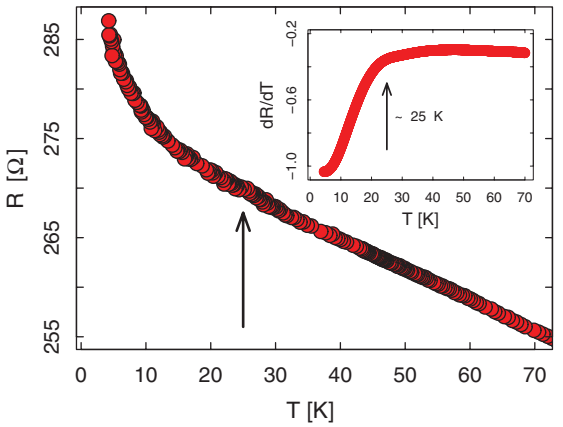

FIG. 8. (Color online) Resistance below 70 K of a thick film of nanographite (Fig. 1) as a function of temperature with weak nonmetallic temperature dependence. It shows a stronger increase below 25 K where the FM interaction is observed by ESR. The $R'(T)$ dependence presented in the inset clearly suggests a change at around 25 K.

on the g factors both for the narrow and broad lines, distinct from simple defects in a CBM (too big for both lines), we would like to suggest the possibility of NMP functionalization induced by sonication. This mechanical energy locally could enhance the probability of the chemical bonding of NMP with the sp^2 network. It is likely the NMP molecules attach preferentially to the sites which are already defected.

The NMP molecules perturb the electronic structure of graphite in the same manner as do vacancies. It is plausible that the stronger spin-orbit coupling of the NMP in respect to carbon gives an overall higher g factor for the assembly.

DFT calculations reveal that hydrogen functionalization leads to the magnetism. However, modeling the functionalization together with NMP is intricate and falls beyond the scope of the present study. Nevertheless, the NMP in graphene can also form covalent bonds to induce magnetism.

Our ESR data can be interpreted in terms of the onset of the two-dimensional (2D) ferromagnetic coupling between the spins emerging due to the H-saturated C atoms. As can be seen from Fig. 7, close to the ordering temperature (hypothetically speaking, $T_C = 0$ K) $\Delta H(T)$ broadens considerably below 25 K.

This type of behavior is generic for a 2D ferromagnet.[32] It is known that the dominant contribution to thermodynamic properties of weak ferro- and antiferromagnets above the transition temperature comes from diffusive magnetic excitations. In 2D systems with FM correlations, the $q = 0$ mode of the fluctuations grows considerably as temperature is lowered towards the critical temperature. In this case, the temperature dependence of ΔH follows the $\langle \hat{S}^z_{q=0} \hat{S}^z_{-q=0} \rangle \sim (k_BT)\chi(T)$ law rather than that of $\langle \hat{S}^z_{q=0} \hat{S}^z_{-q=0} \rangle^{-1}$, which is the case for a 3D ferromagnet.[32] The best fit for the temperature dependence of $\Delta H(T)$ was found to be $\sim 1/T$, thus meaning that as the temperature is lowered from 25 towards 0 K, $\chi(T)$ increases as $T^{-\gamma}$ with $\gamma \approx 2$. The high critical exponent $\gamma \approx 2$ points to the onset of the 2D ferromagnetic coupling. In particular, the Ising model of 2D ferromagnets predicts 7/4 for γ.[33]

Also, using the relation for the in-plane resonance field of 2D ferromagnets,[34] the g-factor temperature dependence below 25 K is given by

$$g(T) = g/\sqrt{1 + 4\pi\chi(T)\rho/M}, \qquad (1)$$

where $M = 12$ g/mol, $\rho = 2.2$ g/cm^3, and $g = 2.011$. Based on Eq. (1), we find that the relative change of g with respect to $g(T)$ obtained at 4.5 K is $\delta g/g \approx 2\pi\chi\rho/M \approx 5 \times 10^{-6}$ $(\chi \gg \chi_{RT})$. The expression in Eq. (1) corroborates only qualitatively the related experimental value $\delta g/g \approx 10^{-2}$. We believe that the discrepancy between the estimated $\delta g/g \approx 5 \times 10^{-6}$ from expression (1) and the experimentally found $\delta g/g \approx 10^{-2}$ might be due to a very rough estimation of $\chi_{\rm RT}$. The corresponding susceptibility has been estimated as 7.5×10^{-8} emu/mol.[35] For example, assuming that $J \sim 50$ K, the temperature dependence of the susceptibility (Fig. 4) becomes consistent with the picture of ferromagnetic correlations at 1D graphene edges,[13] but this picture would then require $\chi_{\rm RT}$ to be nearly three orders of magnitude bigger.

Resistance measurements of the thick film of the nanographite deposit (Fig. 8) signifies also the onset of the FM domains at 25 K. The resistance shows nonmetallic temperature dependence, a weak increase of R with decreasing temperature. This is consistent with a relatively easy hopping between the particles. However, as soon as the FM local order is established in the perturbed regions of the graphite layers, the resistance increases more strongly on lowering the temperature. This observation suggests that the clusters with a local magnetic order are extended structures and that it is not easy to short circuit them with the pristine regions.

If one admits the possibility that functionalization represents the defect sites, which induce magnetic moments in the graphitic structure, one could perform a targeted functionalization of graphene and study the appearance of FM correlations.

ACKNOWLEDGMENTS

The work is supported by the Swiss NSF and its NCCR "MaNEP" and by the European research network Impress. Ž.Š. acknowledges support from the Serbian Ministry of Education and Science under the Grant No. 171033. The assistance of C. Vâju and R. Gaál is gratefully acknowledged.

*dejan.djokic@epfl.ch

[1] P. Avouris, Z. H. Chen, and V. Perebeinos, Nat. Nanotechnol. **2**, 605 (2007).

[2] J. Fernández-Rossier and J. J. Palacios, Phys. Rev. Lett. **99**, 177204 (2007).

[3] Y. W. Son, M. L. Cohen, and S. G. Louie, Nature (London) **444**, 347 (2006).

[4] J. Barzola-Quiquia, P. Esquinazi, M. Rothermel, D. Spemann, T. Butz, and N. García, Phys. Rev. B **76**, 161403(R) (2007).

[5] M. Riccò, D. Pontiroli, M. Mazzani, M. Choucair, J. A. Stride, and O. V. Yazyev, Nano Lett. **11**, 4919 (2011).

[6] P. M. Allemand, K. C. Khemani, A. Koch, F. Wudl, K. Holczer, S. Donovan, G. Grüner, and J. D. Thompson, Science **253**, 301 (1991).

[7] B. Narymbetov, A. Omerzu, V. V. Kabanov, M. Tokumoto, H. Kobayashi, and D. Mihailović, Nature (London) **407**, 883 (2000).

[8] P. Esquinazi, D. Spemann, R. Höhne, A. Setzer, K. H. Han, and T. Butz, Phys. Rev. Lett. **91**, 227201 (2003).

[9] J. Červenka, M. I. Katsnelson, and C. F. J. Flipse, Nat. Phys. **5**, 840 (2009).

[10] M. A. H. Vozmediano, M. P. López-Sancho, T. Stauber, and F. Guinea, Phys. Rev. B **72**, 155121 (2005).

[11] S. R. Power, F. S. M. Guimares, A. T. Costa, R. B. Muniz, and M. S. Ferreira, e-print arXiv:1112.0205v1.

[12] Y. G. Semenov, J. M. Zavada, and K. W. Kim, Phys. Rev. B **84**, 165435 (2011).

[13] O. V. Yazyev and M. I. Katsnelson, Phys. Rev. Lett. **100**, 047209 (2008).

[14] U. Khan, A. O'Neill, M. Lotya, S. De, and J. N. Coleman, Small **6**, 864 (2010).

[15] Y. Hernandez *et al.*, Nat. Nanotechnol. **3**, 563 (2008).

[16] J. J. Mortensen, L. B. Hansen, and K. W. Jacobsen, Phys. Rev. B **71**, 035109 (2005).

[17] J. Enkovaara *et al.*, J. Phys.: Condens. Matter **22**, 253202 (2010).

[18] P. E. Blöchl, Phys. Rev. B **50**, 17953 (1994).

[19] J. P. Perdew, K. Burke, and M. Ernzerhof, Phys. Rev. Lett. **77**, 3865 (1996).

[20] M. Saint Jean, C. Rigaux, and J. Blinowsky, J. Phys. Radium **51**, 1193 (1990).

[21] F. Beuneu, C. l'Huillier, J. P. Salvetat, J. M. Bonard, and L. Forró, Phys. Rev. B **59**, 5945 (1999).

[22] L. Ćirić *et al.* (to be published).

[23] D. L. Huber, R. R. Urbano, M. S. Sercheli, and C. Rettori, Phys. Rev. B **70**, 125417 (2004).

[24] Y. W. Son, M. L. Cohen, and S. G. Louie, Phys. Rev. Lett. **97**, 216803 (2006).

[25] Ž. Šljivančanin, M. Andersen, L. Hornekær, and B. Hammer, Phys. Rev. B **83**, 205426 (2011).

[26] J. Lahiri, Y. Lin, P. Bozkurt, I. I. Oleynik, and M. Batzill, Nat. Nanotechnol. **5**, 326 (2010).

[27] L. Nilsson, Ž. Šljivančanin, R. Balog, T. R. Linderoth, E. Lægsgaard, I. Stensgaard, B. Hammer, F. Besenbacker, and L. Hornekær, Carbon **50**, 2052 (2012).

[28] O. V. Yazyev and L. Helm, Phys. Rev. B **75**, 125408 (2007).

[29] H. A. Mizes and J. S. Foster, Science **244**, 559 (1989).

[30] E. H. Lieb, Phys. Rev. Lett. **62**, 1201 (1989); **62**, 1927(E) (1989).

[31] O. V. Yazyev, Phys. Rev. Lett. **101**, 037203 (2008).

[32] P. M. Richards, *Proceedings of the International School of Physics "E. Fermi" Course LIX*, edited by K. A. Mueller and A. Rigamonti (North-Holland, Amsterdam, 1976), p. 538.

[33] D. B. Abraham, Phys. Lett. A **43**, 163 (1973).

[34] C. Kittel, *Introduction to Solid State Physics*, 4th ed. (Wiley, New York, 1971).

[35] O. Chauvet, G. Baumgartner, M. Carrard, W. Basca, D. Ugarte, W. A. de Heer, and L. Forró, Phys. Rev. B **53**, 13996 (1996).